EFFECTS OF DIFFERENTIAL OSCILLATOR PHASE NOISE IN PRECODING PERFORMANCE

Liz Martínez Marrero[1*], Juan C Merlano Duncan[2], Jorge Querol[3], Symeon Chatzinotas[4], Adriano J Camps Carmona[5], Björn Ottersten[6]

[1,2,3,4,6]SnT, University of Luxembourg, 29 Avenue JF Kennedy, Luxembourg, Luxembourg
[5]Universitat Politècnica de Catalunya, Campus Nord, building D4, office 016, Barcelona, Spain
**liz.martinez-marrero@uni.lu*

Keywords: PHASE NOISE, OSCILLATOR MODEL, LINEAR PRECODING, SYSTEM PERFORMANCE

Abstract

Satellite Precoding is a promising technique to meet the target data rates of the future high throughput satellite systems and the costs per bit as required by 5G applications and networks, but it requires strict synchronization among the transmitted waveforms, in addition to accurate channel state information. Most of the published work about this topic consider ideal oscillators, but in practice, the output of an oscillator is not a single spectral line at the nominal frequency. This paper proposes a model for the oscillator phase noise and analyzes the resulting received signal to interference plus noise ratio (SNIR) in a satellite communication system using Precoding. Simulations of a communication satellite system with a two-beam transponder and two receivers were performed to compute the effective SNIR. This work uses a simulator which also considers practical impairments such as time misalignment, errors in the channel state information, interference, thermal noise and phase noise masks for satellite oscillators. The Precoding methods used for the analysis are Zero Forcing (ZF) and Minimum Mean Square Error (MMSE). The obtained results prove that there is a degradation in the performance due to the use of independent oscillators but this effect is compensated by the precoding matrix.

1 Introduction

Satellite Precoding is a promising strategy to meet the target data rates of the future high throughput satellite systems (HTS) and the costs per bit as required by 5G applications and networks [1], [2]. Recent research activities have a special focus on multi-beam Precoding for multicast communication to achieve higher energy efficiencies [3] and to design better scheduling algorithms [4].

Precoding, which is a multi-user MIMO technique, requires strict synchronization among the transmitted waveforms in addition to channel state information, a requirement shared by all coherent distributed MIMO techniques [5]. A considerable amount of literature introducing new synchronization methods has been published [6]. Besides, other works have analyzed the effects of phase errors on signal coherence [7], [8]. Specifically, authors in [8] consider errors resulting from imperfect clock alignment and platform spatial measurements in an open-loop system. As a result, they obtain beamforming's tolerance to synchronization errors depending on the number of nodes and the desired coherence gain.

The studies mentioned above consider ideal oscillators, but in practice, the output of an oscillator is not a single spectral line at the nominal frequency f_0, but it has sideband power as is shown in Fig 1 [9]. These phase and frequency instabilities affect Precoding performance.

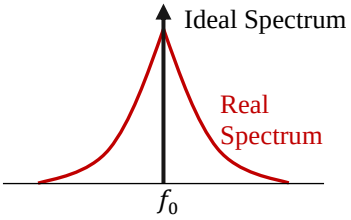

Fig. 1 Spectrum of the oscillator

Using a common local oscillator (LO) as clock reference might seem like a solution to this problem but it is not an alternative in distributed systems, such as network MIMO [10] and cloud radio access network (C-RAN) [4], [11]. In this context, the main challenge is to coordinate the transmission of multiple geographically distant antennas that cannot use a common LO. The lack of a common oscillator also appears in practical satellite systems, due to technical constraints, such as independency between payloads, autonomy, robustness, cross-interference between RF channels and redundancy, where the whole system should not rely on the same oscillator [5], [12].

Some authors have dealt with this problem during Precoding design and implementation. For example, in [13], Gharanjik *et al.* propose a robust design by considering the time-varying phase noise introduced by oscillators onboard the satellite. The robustness is imparted by modeling the phase uncertainty as a random process and ensuring that the outage probability is maintained at desired levels. While in [14], Taricco considers the phase instability of the local oscillators driving the antenna feeds at the satellite payload as one of the phase offset causes in the Precoding implementation. Both papers model the phase uncertainty as Gaussian random process with zero mean and standard deviation σ, $2° < \sigma < 20°$.

A very interesting paper recently explores the effects of non-ideal oscillators in a multi-antenna hybrid digital-analog beamforming transceiver architecture [15]. The authors modeled the phase noise as Wiener and Gaussian processes in

three different architectures: common LO, independent LOs and a block-based architecture. Through simulations they arrived at the conclusion that the phase noise has more impact on the system performance when it is modeled as a Wiener process in an independent LOs architecture. In that case, for a phase noise variance of 10°, there is an error of more than 7° at the beam pointing and the sidelobe level increases in almost 2 dB respect to the common LO architecture.

However, in practice oscillator noise is affected by additional phenomena that are not included in the aforementioned models. Many authors have studied this topic, searching for advanced models to characterize oscillator near-carrier power spectral density (PSD) [16], [17]. Empirical models based on measurements suggest that the phase noise PSD can be described as a sum of power-law processes $h_\alpha|f|^\alpha$ with $\alpha \in \{-4,-3,-2,-1,0\}$ [9]. According to this idea the random walk frequency noise, $h_4|f|^4$, continues increasing infinitely while frequency approaches oscillator's nominal value. However, more recent researches consider an additional Gaussian session segment [16], instead of the spectral line at the carrier frequency shown in Fig. 1, which is more similar to the real characteristic. This model, represented in Fig 2, includes the frequency drifts of a practical system, which is similar to a frequency modulation or spreading of the main carrier.

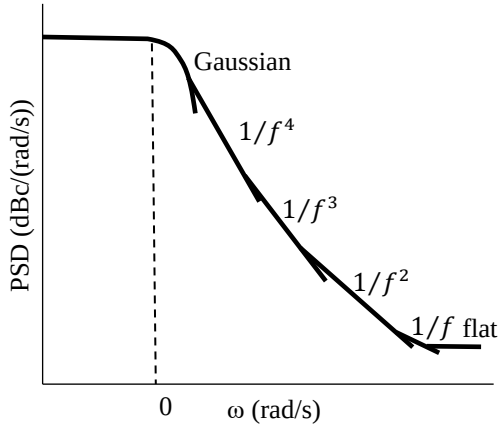

Fig. 2 Oscillator PSD characteristic near the oscillator frequency [16]

In this paper, we propose a model for the oscillator phase noise and analyze the resulting received signal to interference plus noise ratio (SNIR) in a satellite communication system using Precoding. The work takes advantage of the simulations of a system with two beams and two receivers using a simulator developed by the Sigcom group. This allows considering practical impairment sources in a satellite communication such as time misalignment, errors in the channel state information, nonlinearities in the transmitter, interference, thermal noise and phase noise masks for consumer reception systems from ETSI standards for Digital Video Broadcasting (DVB) [19]. The Precoding methods used for the analysis are Zero Forcing (ZF) and Minimum Mean Square Error (MMSE) which are the simplest and most popular among the scientific community. This work analyzes independent LO for each beam and modeled the phase noise according to the two-state model proposed by Galleani in [20].

2 Two-state noise oscillator model

The output voltage $u_0(t)$ of a generic oscillator with a nominal frequency f_0 is $u_0(t) = [A + a(t)]\cos(2\pi f_0 t + \phi(t))$ where A is the mean amplitude of the oscillator output, $a(t)$ is the zero-mean amplitude noise and $\phi(t)$ is an error term due to oscillator phase noise. In this work, we consider that the effects of amplitude noise are overshadowed by the effects of phase noise, which is a common assumption in published work in this field. From this expression, we can obtain two fundamental quantities used to characterize clocks: phase and frequency deviation. The frequency deviation $y(t)$ is defined as the derivative of the phase deviation, which is $x(t) = \frac{\phi(t)}{2\pi f_0}$.

As was mentioned above, phase noise PSD, $S_\phi(f)$, can be described by

$$S_\phi(f) = \begin{cases} \sum_{\alpha=-4}^{0} h_\alpha f^\alpha & 0 < f < f_h \\ 0 & f \geq f_h \end{cases} \quad (1)$$

where f_h is the high-frequency cut-off of an infinitely sharp low-pass filter [21]. These $h_\alpha f^\alpha$ terms are related to random walk FM, flicker FM, white FM, flicker and white phase noise respectively [16].

A simpler implementation is the two-state clock noise model which considers just white FM phase noise ($\alpha = -2$) and random walk FM phase noise ($\alpha = -4$). Experimental evidence shows that the frequency deviation of a cesium clock is made by these two noises, namely, a white noise and a Wiener process. The last one is responsible for the random walk nature of the frequency deviation, while the white noise accounts for the local oscillations. Therefore, the frequency deviation can be written as

$$y(t) = \xi_1(t) + x_2(t) \quad (2)$$

where $\xi_1(t)$ denotes a zero-mean Gaussian random process, $\xi_1(t) \sim N(0, q_1)$, and $x_2(t)$ is a Wiener process.

The Wiener process, also known as Brownian motion, is the prototype of random walks. It is characterized because the increments between two consecutive samples are normally distributed independent processes, $\Delta w \sim N(0, t)$. In continuous time:

$$x_2(t) = \int_0^t \xi_2(\dot{t})\, d\dot{t} \quad (3)$$

where $\xi_2(\dot{t}) \sim N(0, q_2)$.

To obtain the two-state model of the phase noise we substitute in equation (2) the phase deviation and the expression (3) for the Wiener process:

$$\frac{dx(t)}{dt} = \xi_1(t) + \int_0^t \xi_2(\dot{t})\, d\dot{t} \quad (4)$$

Taking the derivative for both sides:

$$x(t) = x_1(t) = \int_0^t \xi_1(\check{t}) + \int_0^t \xi_2(\dot{t})\, d\dot{t} d\check{t} \quad (5)$$

Equation (5), shown in graphical form in Fig 3, describes the two-state clock noise model [17].

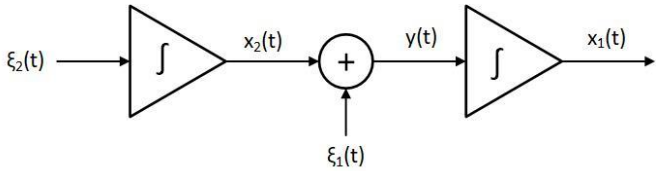

Fig. 3 Two-state noise clock model

2.1 Discrete-Time Implementation

To implement the system in Fig 3, it is useful to express equation (4) in the state-space form:

$$\begin{bmatrix} \boldsymbol{x'_1}(t) \\ \boldsymbol{x'_2}(t) \end{bmatrix} = \begin{bmatrix} 0 & 1 \\ 0 & 0 \end{bmatrix} \begin{bmatrix} \boldsymbol{x_1}(t) \\ \boldsymbol{x_2}(t) \end{bmatrix} + \begin{bmatrix} \boldsymbol{\xi_1}(t) \\ \boldsymbol{\xi_2}(t) \end{bmatrix} \quad (6)$$

Where the inputs $\boldsymbol{\xi_1}$ and $\boldsymbol{\xi_2}$ are two independent zero-mean Gaussian random processes with a correlation matrix $\boldsymbol{R}_{\xi_1\xi_2}(\tau) = \begin{bmatrix} q_1 & 0 \\ 0 & q_2 \end{bmatrix} \delta(t)$; $\boldsymbol{x_1}$ and $\boldsymbol{x_2}$ are the states and $\boldsymbol{x'_1}$, $\boldsymbol{x'_2}$ refers to their derivatives [17].

A discrete-time equivalent expression for equation (6) was obtained in [20] and has the form:

$$\boldsymbol{x}[n] = \begin{bmatrix} 1 & T_s \\ 0 & 1 \end{bmatrix} \boldsymbol{x}[n-1] + \boldsymbol{\eta}[n-1] \quad (7)$$

with $\boldsymbol{x}[n] = \begin{bmatrix} \boldsymbol{x_1}[n] \\ \boldsymbol{x_2}[n] \end{bmatrix}$, $\boldsymbol{\eta}[n] = \begin{bmatrix} \boldsymbol{\eta_1}[n] \\ \boldsymbol{\eta_2}[n] \end{bmatrix}$ and T_s sampling period. The covariance matrix of $\boldsymbol{\eta}[n]$ is given by

$$\boldsymbol{C}_{\boldsymbol{\eta_1},\boldsymbol{\eta_2}} = \begin{bmatrix} q_1 T_s + q_2 \dfrac{{T_s}^3}{3} & q_2 \dfrac{{T_s}^2}{2} \\ q_2 \dfrac{{T_s}^2}{2} & q_2 T_s \end{bmatrix} \quad (8)$$

According to [20], [22], q_1 and q_2 are directly related to the Allan variance $\sigma_y^2(\tau)$ through

$$\sigma_y^2(\tau) = \frac{q_1}{\tau} + \frac{q_2 \tau}{3} \quad (9)$$

This is a typical tool used to characterize the noise in oscillators and could be obtained from experimental measurements. Besides, the Allan variance is related to the noise PSD in equation (1) by [21]

$$\begin{aligned} \sigma_y^2(\tau) = h_{-4} \frac{2\pi^2}{3} \tau + h_{-3} 2 \ln 2 + h_{-2} \frac{1}{2\tau} \\ + h_{-1} \frac{1.038 + 3\ln(2\pi f_h \tau)}{4\pi^2 \tau^2} \\ + h_0 \frac{3 f_h}{4\pi^2 \tau^2} \end{aligned} \quad (10)$$

For the two-state model analyzed in this paper, we consider just the first and the third terms in equation (10). Then, equalling equation (9) and (10) we obtain

$$\begin{aligned} q_1 &= \frac{h_{-2}}{2} \\ q_2 &= 2\pi^2 h_{-4} \end{aligned} \quad (11)$$

Using these equivalences it can be generated the two-state model for any real or theoretical phase noise PSD.

3 Satellite precoding system with different clock references

This work studies the effects of the oscillators phase noise in a satellite precoding system detailed in the next section. To simplify the analysis, unicast communication between the satellite and two user terminals on Earth is considered. The satellite has two antennas feeds in single feed per beam configuration and uses precoding to avoid interference between the beams.

It is well known that precoding operates by generating the transmitted signal $\chi(t)$ by multiplying the input symbol vector with the precoding matrix $\boldsymbol{W} = \begin{bmatrix} w_{11} & w_{12} \\ w_{21} & w_{22} \end{bmatrix}$. In a vector form:

$$\boldsymbol{\chi_p} = \boldsymbol{W}\boldsymbol{s} \quad (12)$$

Where $\boldsymbol{\chi_p}[n] = \begin{bmatrix} \boldsymbol{\chi_{p1}} \\ \boldsymbol{\chi_{p2}} \end{bmatrix}$ is the precoded transmitted signal and $\boldsymbol{s}[n] = \begin{bmatrix} \mathbf{s_1} \\ \boldsymbol{s_2} \end{bmatrix}$ represents the input data symbols. It should be noted that the phase noise is a fast-varying process that cannot be captured in the CSI loop. To evaluate the error introduced by different clock references during the upconversion, the terms $e^{j\phi(t)}$ were included in equation (12):

$$\begin{bmatrix} \boldsymbol{\chi_{p1}} \\ \boldsymbol{\chi_{p2}} \end{bmatrix} = \begin{bmatrix} w_{11} e^{j\boldsymbol{\phi_1}} & w_{12} e^{j\boldsymbol{\phi_1}} \\ w_{21} e^{j\boldsymbol{\phi_2}} & w_{22} e^{j\boldsymbol{\phi_2}} \end{bmatrix} \begin{bmatrix} \mathbf{s_1} \\ \boldsymbol{s_2} \end{bmatrix} \quad (13)$$

The precoding matrix is calculated using the channel state information (CSI) obtained from each receiver. Basically, each user sends its estimation of the downlink channel $\widetilde{\boldsymbol{H}}$, and the precoding matrix is calculated in the gateway by two methods: zero-forcing (ZF) or minimum mean square error (MMSE). The former uses the pseudo-inverse of the channel matrix, $\boldsymbol{W} = \widetilde{\boldsymbol{H}}^H (\widetilde{\boldsymbol{H}} \widetilde{\boldsymbol{H}}^H)^{-1}$, where $\widetilde{\boldsymbol{H}}^H$ means the Hermitian matrix of $\widetilde{\boldsymbol{H}}$. Otherwise, MMSE takes into account both the interference and the noise in order to improve the system performance also in noise-limited scenarios, $\boldsymbol{W} = \widetilde{\boldsymbol{H}}^H (\widetilde{\boldsymbol{H}} \widetilde{\boldsymbol{H}}^H + \alpha \boldsymbol{I})^{-1}$, with α being a regularization parameter inversely proportional to the SNR and $\boldsymbol{I}$ the identity matrix [23].

The received signal at the user terminal equals

$$\boldsymbol{r} = \boldsymbol{H}\boldsymbol{\chi_p} + \boldsymbol{z} \quad (14)$$

where $\boldsymbol{z}[n] = \begin{bmatrix} \mathbf{z_1} \\ \boldsymbol{z_2} \end{bmatrix}$ is the Gaussian noise and $\boldsymbol{H} = \begin{bmatrix} h_{11} & h_{12} \\ h_{21} & h_{22} \end{bmatrix}$ is the experienced channel on the downlink. It should be noted that in a system with a common clock reference (phase drift $e^{j\boldsymbol{\phi}}$), instant and perfect channel estimation ($\widetilde{\boldsymbol{H}} = \boldsymbol{H}$), then applying ZF yields $\boldsymbol{W} = \boldsymbol{H^{-1}}$ and $\boldsymbol{r} = \boldsymbol{s}e^{j\boldsymbol{\phi}} + \boldsymbol{z}$. However, substituting equation (13) in (14)

$$\begin{bmatrix} \boldsymbol{r_1} \\ \boldsymbol{r_2} \end{bmatrix} = \begin{bmatrix} g_{11}\boldsymbol{s_1} + g_{12}\boldsymbol{s_2} + \boldsymbol{z_1} \\ g_{21}\boldsymbol{s_1} + g_{22}\boldsymbol{s_2} + \boldsymbol{z_2} \end{bmatrix} \quad (15)$$

With

$$\begin{aligned} g_{11} &= \frac{(h_{11}h_{22}e^{j\boldsymbol{\phi_1}} - h_{12}h_{21}e^{j\boldsymbol{\phi_2}})}{\det(\boldsymbol{H})} \\ g_{12} &= \frac{(h_{12}h_{11}e^{j\boldsymbol{\phi_2}} - h_{11}h_{12}e^{j\boldsymbol{\phi_1}})}{\det(\boldsymbol{H})} \\ g_{21} &= \frac{(h_{21}h_{22}e^{j\boldsymbol{\phi_1}} - h_{22}h_{21}e^{j\boldsymbol{\phi_2}})}{\det(\boldsymbol{H})} \\ g_{22} &= \frac{(h_{22}h_{11}e^{j\boldsymbol{\phi_2}} - h_{21}h_{12}e^{j\boldsymbol{\phi_1}})}{\det(\boldsymbol{H})} \end{aligned}$$

One of the most used parameters to measure performance in precoding systems is the signal to noise plus interference ratio (SNIR). According to [24], the SNIR at each receiver when ZF is used can be computed as:

$$SNIR_i = \frac{|g_{ii}|^2}{|g_{ij}|^2 + {\sigma_z}^2} \quad (16)$$

This equation considers channel noise power $\sigma_z{}^2$ and interference power $|g_{ij}|^2$. It is evident that the use of different clock references will decrease the SNIR at the receivers due to an increment in the interference between beams. A similar approach can be followed for MMSE but it is omitted here due to space limitations.

4 System implementation

The satellite communication system simulated is represented in Fig 4. The system is composed of a two-beams transparent satellite transponder, the communication channel and the ground segment with the gateway and two user terminals. The transmitted signal was simulated according to the framing structure in the DVB-S2x standard [25]. Precoding is used for the downlink communication between the transponder and the user terminals, identified as Rx_1 and Rx_2 in Fig 4. The channel is assumed static in all simulations, and the return and feeder links are considered ideal. The right side of Fig 4, represents how was included the oscillator model in the simulations: $u_1(t)$ and $u_2(t)$ are the clock reference for each beam at the transponder. Section 5 analyzes the effects of using two independent oscillators, as shown in Fig 4, against the use of a common clock reference, $\boldsymbol{u_1(t) = u_2(t) = u(t)}$.

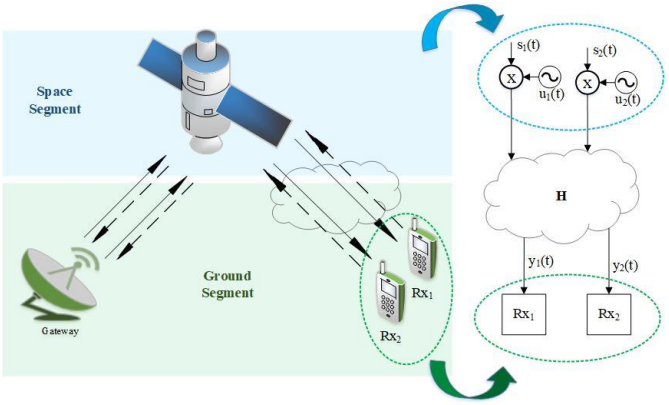

Fig. 4 Simplified diagram of a satellite communication system using Precoding with independent clock references for each beam in the downlink channel.

The standard DVB-S2x defines a fixed framing structure to increase resilience to co-channel interference and to support synchronization algorithms [25]. For precoding purposes, the specifications state 9 bundled payload frames at each superframe. Each bundled frame contains a header, a precoded pilot field, 71 non-precoded pilots and 64800 payload symbols. This structure is represented in Fig 5. In the performed simulations, it was considered 80 MBaud of baud rate. Then, the transmission of a pilot takes 0.45 µs while a superframe lasts for 7.66 ms.

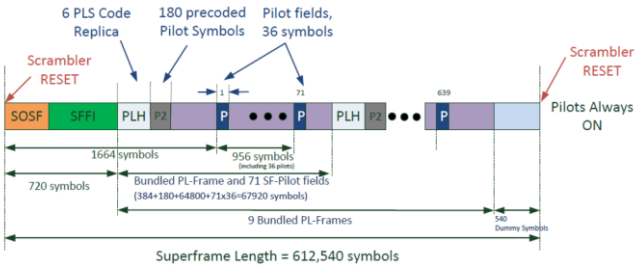

Fig. 5 Superframe structure from the DVB-S2x standard [25]

Precoding systems use non-precoded pilots to estimate the channel response at the receivers. Each pilot is formed by 36 BPSK symbols carrying Walsh-Hadamard sequences. The receivers compute an estimation of the distortion introduced at each beam by the channel. This information is sent to the Gateway, where the CSI, $\tilde{\boldsymbol{H}} = \begin{bmatrix} \tilde{h}_{11} & \tilde{h}_{12} \\ \tilde{h}_{21} & \tilde{h}_{22} \end{bmatrix}$, is estimated. In order to increase robustness, the receiver averages over $\tilde{\boldsymbol{H}}$ estimates originating from several consecutive pilot sequences. The number of averaged estimates varies according to the SNIR of the system. The simulations, evaluate different values for this parameter.

The gateway uses these CSI to calculate the precoding matrix. There are multiple algorithms to calculate $\boldsymbol{W}$, but this work uses only ZF and MMSE, which are well known by the community. It is worth noting that the estimation from one superframe is used to compute the precoding matrix for the next superframes. The time gap between both of them depends on the delay of the communication link. For the simulations, it is considered zero-delay and 500 ms, which is the approximate delay for a closed-loop between the ground and a GEO satellite. Closed-loop includes both links, the direct one, gateway-transponder-receivers, shown as solid line arrows in Fig 4, and the return link, receivers-transponder-gateway, with dashed line arrows.

The gateway-satellite link is considered ideal, which is a valid assumption since it is usually a direct link with frequency division multiplexing and high SNIR. However, it introduces a considerable delay that cannot be omitted. For that reason, it was included in the channel model the response of the link between the satellite and the user terminals and the delay of both sections gateway-satellite and satellite-user terminals. The channel is modeled with coefficients $\boldsymbol{h_{ij}}$ provided through an European Space Agency (ESA) project [18]. The channel coefficients used for the selected locations are

$$\boldsymbol{H} = \begin{bmatrix} -0.4016 + 0.0064j & -0.0071 + 0.0277j \\ -0.1911 - 0.1533j & -0.2501 - 0.3269j \end{bmatrix} \cdot 10^{-6}$$

5 Simulations results

Fig 6 shows two realizations, 8.4 s, of the phase noise model implemented. They were used to generate the phase drift at each clock reference in the satellite. As was discussed in

section 2, the phase noise model output contains a Wiener process plus an integrated Wiener process. That makes the phase noise have a smoother behavior than that of a simple Wiener process, so its variance grows quadratically with time, while the variance of a Wiener process increases linearly with time.

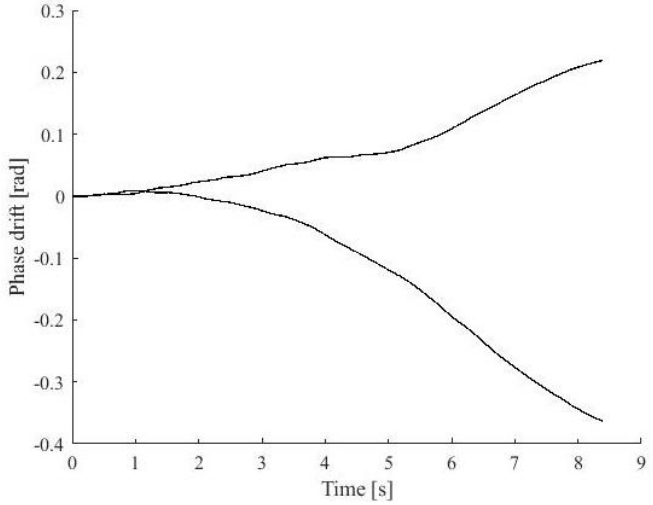

Fig. 6 Phase drift from two independent oscillators

The phase noise model output is a non-stationary stochastic process which implies that its PSD varies with time. The time-frequency representation of this PSD is shown in Fig 7.

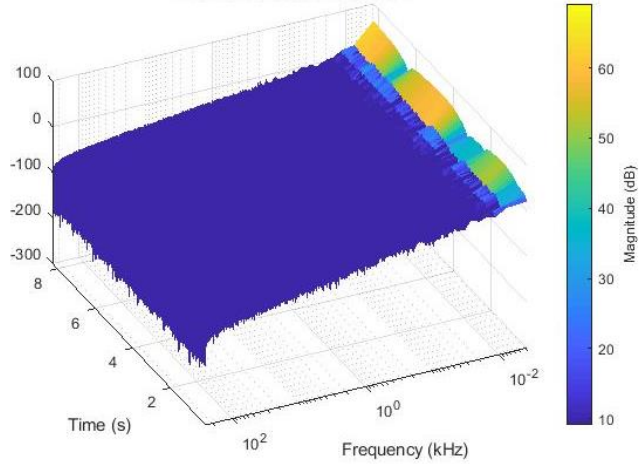

Fig. 7 Time-frequency representation of the spectral characteristic for one realization of the phase noise.

Besides, it was computed the estimation of the PSD represented in Fig 7 to verify the correspondence with the desired phase noise mask. The phase noise masks are generated through measurements of real oscillators PSD. For the simulations, a PSD with the $1/f^2$ starting in 10 Hz at -75 dB was chosen. Figure 8 shows the estimated PSD of the clock references used in the simulations.

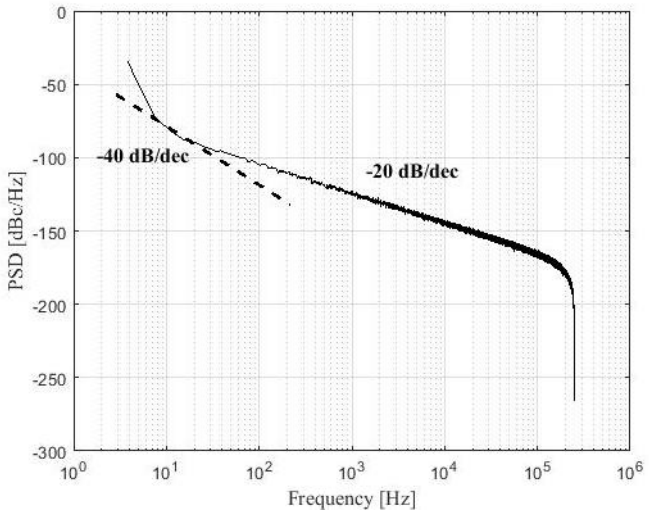

Fig. 8 Estimated PSD for the phase noise used in the simulations.

The first simulation models the performance degradation due to the phase noise in an ideal system with perfect and updated CSI. It was compared the SNIR obtained with ZF and MMSE for a range of transmission power when it is used a common clock reference, dashed lines in Fig 9, against independent oscillators for each beam, solid line in Fig 9. As can be seen in the figure, there is an SNIR gap that grows with the transmission power. That is an expected result since the interference in equation (16) is directly related to the transmission power. It means that for low transmission power the channel noise $\sigma_z{}^2$ has more influence in the system performance, but as the transmission power increases the system is more affected by the inter-beam interference due to the oscillators phase noise. However, the SNIR degradation is lower than 4 dB in the worse scenario.

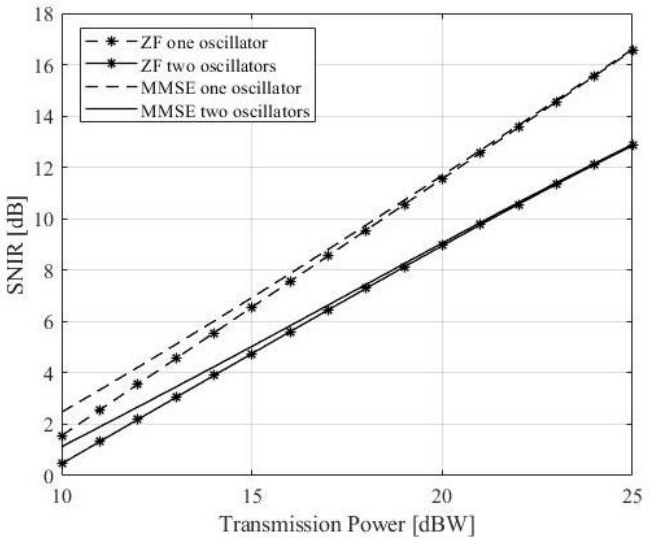

Fig. 9 Open-loop simulation of phase noise PSD.

Besides, the closed-loop system was modeled: first, CSI is estimated using the pilots from three superframes and with this estimation, the system calculates the precoding matrix to send the payload symbols of the next superframe. It was considered zero and 500 ms of delay and it was computed the SNIR at the

receivers for a set of transmission power. The results are shown in Fig 11.

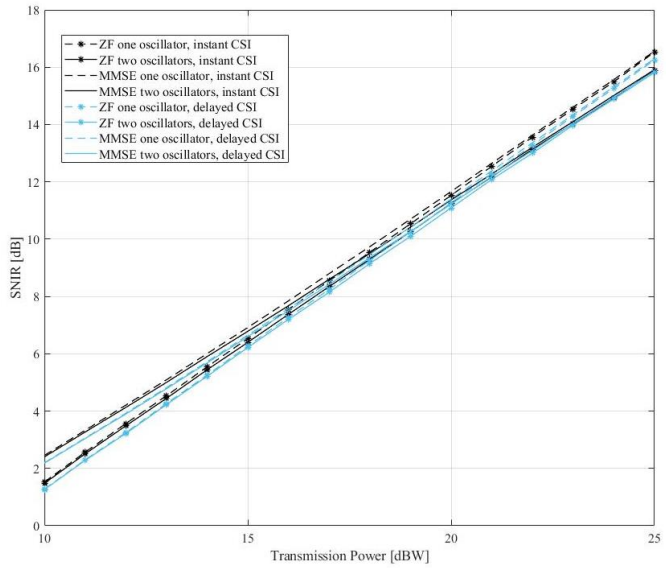

Fig. 11 Closed-loop simulation of phase noise PSD.

This simulation shows similar results to the open-loop one, for low transmission power MMSE performs better than ZF and the use of a common oscillator has less impact. However, for higher transmission power the closed-loop showed better results since all curves converge to the same value. This is an expected result since phase deviation due to the oscillators are part of the CSI estimated by the receivers and therefore they are compensated with $\boldsymbol{W}$. The delay has a very small effect in this performance, but it is important to note that this simulation considers a static communication channel. Results may be different when we include the dynamic behavior of the channel.

5 Conclusion

This paper deals with the effects of the phase noise from oscillators in the performance of satellite communication systems with precoding. Using the two-state phase noise model it was analyzed the degradation in the SNIR at the receivers for a 2x2 system with common and independent clock references. The simulations included the effects of the delay and the CSI estimation errors.

The obtained results prove that there is a degradation in the performance of precoding systems due to the use of independent oscillators. In the open-loop system, the SNIR gap between a common clock reference and independent oscillators increases with the transmission power but never was bigger than 4 dB. However, in a closed-loop system, this effect is compensated by the calculation of the precoding matrix. According to the simulation results, the delay does not have much impact, but it may change if we include the dynamic characteristic of the channel which is part of our future work.

Other open questions in this work are the effect of other impairments such as the initial phase offset between oscillators and the extension to more complex systems, bigger than 2x2.

Acknowledgements

This work was supported by the Fond National de la Recherche Luxembourg, under the CORE project COHESAT: Cognitive Cohesive Networks of Distributed Units for Active and Passive Space Applications.

6 References

[1] R. T. Schwarz, T. Delamotte, K.-U. Storek, and A. Knopp, “MIMO Applications for Multibeam Satellites,” *IEEE Trans. Broadcast.*, pp. 1–18, 2019.

[2] N. Fatema, G. Hua, Y. Xiang, and S. Member, “Massive MIMO Linear Precoding : A Survey,” *IEEE Syst. J.*, vol. 12, no. 4, pp. 3920–3931, 2018.

[3] C. Qi and X. Wang, “Precoding Design for Energy Efficiency of Multibeam Satellite Communications,” *IEEE Commun. Lett.*, vol. 22, no. 9, pp. 1826–1829, Sep. 2018.

[4] Q. Hou, S. He, Y. Huang, H. Wang, and L. Yang, “Joint user scheduling and hybrid precoding design for MIMO C-RAN,” in *2017 9th International Conference on Wireless Communications and Signal Processing, WCSP 2017 - Proceedings*, 2017, vol. 2017-Janua, pp. 1–6.

[5] M. A. Vazquez *et al.*, “Precoding in Multibeam Satellite Communications: Present and Future Challenges,” *IEEE Wirel. Commun.*, vol. 23, no. December, pp. 88–95, 2016.

[6] S. Jayaprakasam, S. K. A. Rahim, and C. Y. Leow, “Distributed and Collaborative Beamforming in Wireless Sensor Networks: Classifications, Trends, and Research Directions,” *IEEE Commun. Surv. Tutorials*, vol. 19, no. 4, pp. 2092–2116, 2017.

[7] F. Quitin, A. T. Irish, and U. Madhow, “A Scalable Architecture for Distributed Receive Beamforming: Analysis and Experimental Demonstration,” *IEEE Trans. Wirel. Commun.*, vol. 15, no. 3, pp. 2039–2053, Mar. 2016.

[8] J. A. Nanzer, R. L. Schmid, T. M. Comberiate, and J. E. Hodkin, “Open-Loop Coherent Distributed Arrays,” *IEEE Trans. Microw. Theory Tech.*, vol. 65, no. 5, pp. 1662–1672, May 2017.

[9] J. Rutman, “Characterization of Phase and Frequency Instabilities in Precision Frequency Sources: Fifteen Years of Progress.,” *Proc. IEEE*, vol. 66, no. 9, pp.

1048–1075, 1978.

[10] C. Song and Y. Jeon, “Weighted MMSE Precoder Designs for Sum-Utility Maximization in Multi-User SWIPT Network-MIMO with Per-BS Power Constraints,” *IEEE Trans. Veh. Technol.*, vol. 67, no. 3, pp. 2809–2813, 2018.

[11] G. Femenias and F. Riera-Palou, “Multi-Layer Downlink Precoding for Cloud-RAN Systems Using Full-Dimensional Massive MIMO,” *IEEE Access*, vol. 6, pp. 61583–61599, 2018.

[12] Y. Yang, W. Wang, and X. Gao, “Distributed RZF Precoding for Multiple-Beam MSC Downlink,” *IEEE Trans. Aerosp. Electron. Syst.*, vol. 54, no. 2, pp. 968–977, 2018.

[13] A. Gharanjik, M. R. Bhavani Shankar, P. D. Arapoglou, M. Bengtsson, and B. Ottersten, “Robust precoding design for multibeam downlink satellite channel with phase uncertainty,” in *ICASSP, IEEE International Conference on Acoustics, Speech and Signal Processing - Proceedings*, 2015, vol. 2015-August, pp. 3083–3087.

[14] G. Taricco, “Linear Precoding Methods for Multi-Beam Broadband Satellite Systems,” in *European Wireless 2014; 20th European Wireless Conference; Proceedings of*, 2014, pp. 1–6.

[15] Mubarak Umar Aminu, J. Lehtomäki, and Markku Juntti, “Beamforming and Transceiver Optimization with Phase Noise for mmWave and THz Bands,” in *16th International Symposium on Wireless Communication Systems ISWCS 2019*, 2019.

[16] A. Chorti and M. Brookes, “A spectral model for RF oscillators with power-law phase noise,” *IEEE Trans. Circuits Syst. I Regul. Pap.*, vol. 53, no. 9, pp. 1989–1999, 2006.

[17] J. Mcneill, S. Razavi, K. Vedula, and D. Richard, “Experimental Characterization and Modeling of Low-Cost Oscillators for Improved Carrier Phase Synchronization,” in *2017 IEEE International Instrumentation and Measurement Technology Conference (I2MTC)*, 2017.

[18] “LiveSatPreDem – Live Satellite Precoding Demonstration.” [Online]. Available: https://wwwfr.uni.lu/snt/research/sigcom/projects/livesatpredem_live_satellite_precoding_demonstration. [Accessed: 11-May-2019].

[19] ETSI, “Digital Video Broadcasting (DVB); Second generation framing structure, channel coding, and modulation systems for Broadcasting, Interactive Services, News Gathering and other broadband satellite applications; Part 1: DVB-S2,” vol. 1. pp. 1–80, 2014.

[20] L. Galleani, “A tutorial on the two-state model of the atomic clock noise,” *Metrologia*, vol. 45, no. 6, 2008.

[21] *1139-2008 IEEE Standard Definitions of Physical Quantities for Fundamental Frequency and Time Metrology--Random Instabilities.*

[22] C. Zucca and P. Tavella, “The clock model and its relationship with the Allan and related variances,” *IEEE Trans. Ultrason. Ferroelectr. Freq. Control*, vol. 52, no. 2, pp. 289–296, Feb. 2005.

[23] M. Alodeh *et al.*, “Symbol-level and Multicast Precoding for Multiuser Multiantenna Downlink: A State-of-the-art, Classification and Challenges,” *IEEE Commun. Surv. Tutorials*, 2018.

[24] S. Chatzinotas, B. Ottersten, and R. de Gaudenzi, “7.2 multiuser MIMO communications,” in *Cooperative and Cognitive Satellite Systems*, vol. 1, Elsevier Science & Technology, 2015, pp. 220–224.

[25] S. Andrenacci, A. V. Coralli, and G. E. Corazza, “Next Generation Waveforms for Improved Spectral Efficiency. Synchronization and Estimation Techniques Design and Assessment for DVB-S2x Multibeam Systems (TN3-v31),” 2014.